Formation of graphene nanoribbons on the macrofacets of vicinal 6*H*-SiC(0001) surfaces

Kohei Fukuma,[1] Anton Visikovskiy,[1] Takushi Iimori,[2] Toshio Miyamachi,[2] Fumio Komori,[2] and Satoru Tanaka[1,*]
[1]*Department of Applied Quantum Physics and Nuclear Engineering, Kyushu University, Fukuoka 819-0395, Japan*
[2]*Institute for Solid State Physics, The University of Tokyo, Kashiwa, Chiba 277-8581, Japan*

(Received 25 October 2021; revised 5 October 2022; accepted 18 November 2022; published 9 December 2022)

Thermal decomposition of vicinal 6*H*-SiC(0001) surfaces with miscut angles toward the $[1\bar{1}00]$ direction results in the appearance of pairs of (0001) macroterraces and $(1\bar{1}0n)$ macrofacets covered with graphene, as follows. A carpetlike carbon layer grows on the surface, covering both the macroterraces and macrofacets; it forms a $(6\sqrt{3} \times 6\sqrt{3})$ buffer layer on the former ones, whereas its partial periodic bonding with the SiC steps on the latter ones generates a pseudographene nanoribbon (pseudo-GNR) array. The nanoribbons have a width of 1.7–1.8 nm and are aligned in the $[11\bar{2}0]$ direction with a spatial periodicity of 3.3 nm. Scanning tunneling spectroscopy at a nanoribbon indicated a 0.4–0.5 eV energy gap and the Raman spectroscopy analysis of the pseudo-GNR array showed the absence of the 2*D* peak and the polarization dependence of the *G* and *D* peaks, which is typical of the armchair-edge nanoribbon.

DOI: 10.1103/PhysRevMaterials.6.124003

I. INTRODUCTION

Graphene is a two-dimensional material with exotic electronic properties and very high carrier mobility, which makes it an interesting candidate for next-generation electronics [1,2]. Application in traditional logic switching devices, however, requires a band gap that normal graphene lacks. Therefore, methods for opening a gap in the graphene band structure have been investigated. For example, cutting graphene into graphene nanoribbons (GNRs) with armchair edges can generate a substantial energy gap, but the ribbon width must be accurately controlled [3,4]. Lithography [5] and unzipping carbon nanotubes [6] are traditional top-down approaches to fabricate GNRs, while bottom-up approaches include GNR synthesis from molecular precursors [7,8]. Both strategies present some drawbacks, though; the top-down approaches struggle with accurate control of width and edge quality, while the bottom-up ones require specific metal substrates (i.e., the requirement of postgrowth transfer procedure) and suffer in the ribbon alignment.

Today, GNR growth on semiconductor SiC substrates is attracting attention as a new bottom-up method [9–16]. Through molecular beam epitaxy, an array of GNRs having ∼5 nm width can be grown on the nanoperiodic structure [17,18] formed on a vicinal SiC substrate [9]; the resulting GNRs are periodic with ∼10 nm spatial interval and exhibit a band gap of 0.14 eV, as observed via angle-resolved photoemission spectroscopy (ARPES). Graphene grown on a trench or mesa structures premade on SiC(0001) surfaces has also been studied [10–15]. The edge structure of GNRs grown on a trench sidewall is controlled by trench orientation; specifically, the GNRs having zigzag edges grown on the sidewall along the $[1\bar{1}00]$ direction of 6*H*-SiC(0001) surfaces show the characteristics of ballistic conduction [10,11]. Furthermore, both the zigzag-edge GNRs grown on the sidewall of 4*H*-SiC(0001) surfaces [12] and the armchair-edge ones grown on 6*H*-SiC(0001) surfaces [13] exhibit band gaps.

All in all, the growth of very narrow GNRs (of nanometer width) on a semiconductor surface with good uniformity, sufficient width control, and aligned within large arrays (which could be beneficial for device fabrication) has not been achieved yet.

We have previously studied the formation and growth mechanism of graphene on terrace-facet periodic structures (reported as macrostep formation on vicinal SiC(0001) surfaces [19,20]). Step bunching during thermal decomposition results in the formation of macroterraces and macrofacets with a period of several-hundred nanometers. Ienaga *et al.* [21] investigated bilayer graphene formed on macrofacets and observed the periodic modulation of electron-phonon coupling in the top graphene layer via scanning tunneling spectroscopy. This result suggests that the bottom carbon layer is not continuous graphene, but an array of GNRs.

In the present work, we grew a uniform single graphitic layer on macrofacets (hereafter defined as facet graphene) and studied its structure and physical properties. This facet graphene was attached periodically to the underlying substrate structures, and this repetition of freestanding portions of the carbon layer and those bonded to the substrate formed a pseudo-GNR array. The scanning tunneling microscopy/spectroscopy (STM/STS) and Raman analyses revealed features that are characteristic of armchair-edge GNRs with a width of several nanometers.

II. EXPERIMENT

A 6*H*-SiC(0001) substrate with a 15° miscut angle toward the $[1\bar{1}00]$ direction was used to grow the GNR array. Such

*stanaka@nucl.kyushu-u.ac.jp

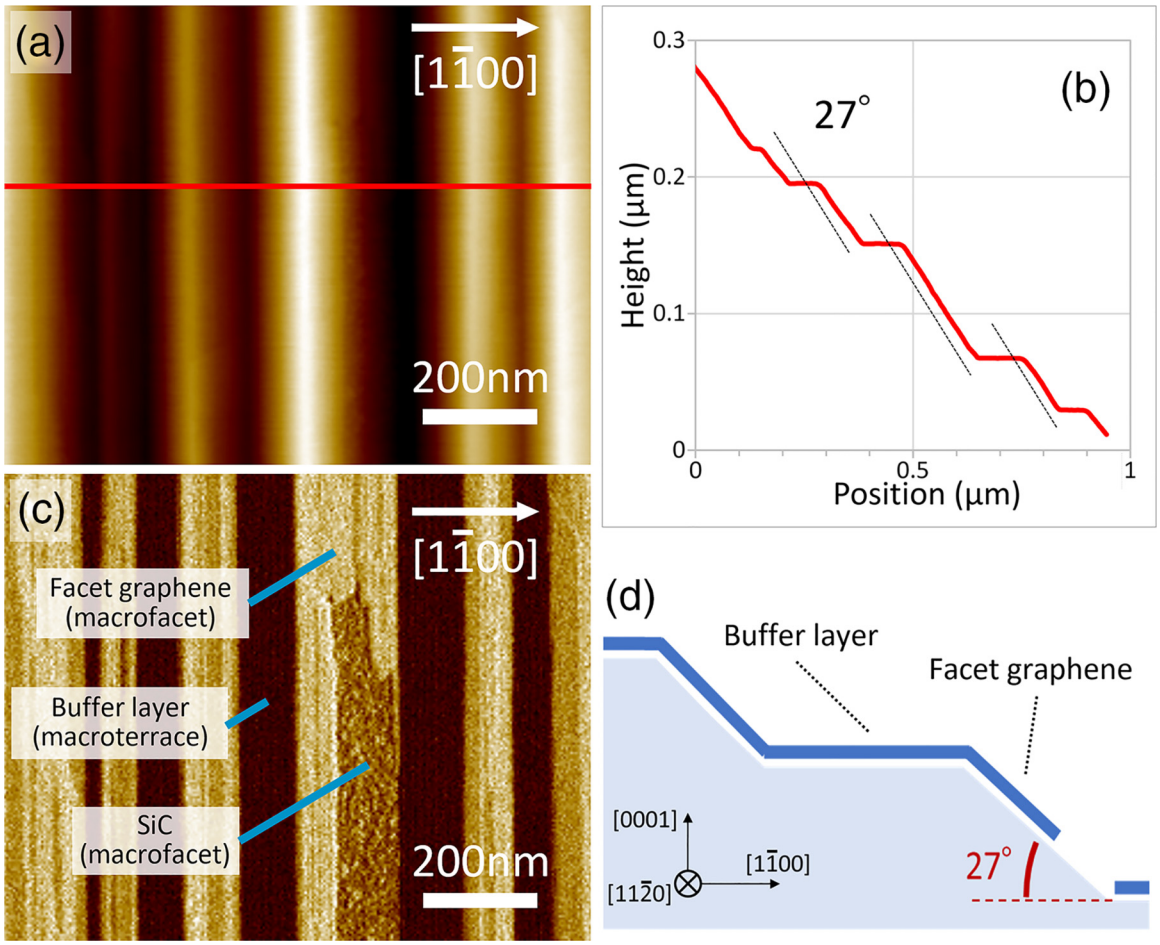

FIG. 1. AFM results on the 15° miscut angle sample. (a) Height and (c) phase images of the sample after surface decomposition. (b) Cross-sectional height profile along the red line in (a); the gray dashed line represents the 27° angle from the (0001) plane. (d) A schematic diagram of the macroterrace-macrofacet structure after facet graphene growth.

a large miscut angle was used to ensure a large facet/terrace area ratio, which is important for surface characterization via macroprobe methods such as low-energy electron diffraction (LEED), ARPES, and Raman; besides, the resulting lower facet angle with respect to the sample surface is more accessible for scanning probe methods due to less interference between tip sidewalls and high-angle facets. The STM/STS and the LEED study have also been carried out on the more common 4° miscut sample, with virtually identical general results except for a much lower facet/terrace area ratio. First, the samples were cleaned and etched via high-temperature annealing (1360 °C) in a hydrogen flow under atmospheric pressure. After confirming by atomic force microscopy (AFM) the surface morphology and the absence of polishing damage, we proceeded with surface thermal decomposition in an Ar atmosphere at ambient pressure and 1500 °C; this treatment led to step bunching, resulting in a periodic surface morphology consisting of (0001) macroterraces and macrofacets [typically 27° inclined with respect to (0001)]. The samples were then analyzed by AFM, LEED, STM/STS, and micro-Raman spectroscopy. STM/STS measurements have been carried out in the Omicron LT-STM system at 77 K using a chemically etched tungsten tip. dI/dV STS measurements have been done using a lock-in amplifier tuned to 730 Hz with 20 ms integration time for each point and averaging several spectrum sweeps.

III. RESULTS AND DISCUSSION

The AFM observation of the sample surface after thermal decomposition [Fig. 1(a)] showed pairs of macroterraces and macrofacets, which had individual widths ranging from tens to ∼200 nm, along the [1$\bar{1}$00] direction. The corresponding cross-sectional profile [Fig. 1(b)] revealed that the macrofacets formed an angle ∼27° with respect to the (0001) macroterraces.

In the AFM phase image [Fig. 1(c)] of the same area, three types of regions of different contrast could be clearly distinguished: dark areas on the macroterraces represent an insulating carbon $(6\sqrt{3} \times 6\sqrt{3})R30°$ buffer layer (hereafter denoted as 6R3) [22–24], while bright and grainy mid-tone areas on macrofacets are ones paved and unpaved by graphene, respectively. The facet's 27° angle, as shown in the schematic cross section [Fig. 1(d)], does not depend on surface miscut and is related to the most energetically stable configuration, as reported in previous studies [14,21]. We will focus on the facet structures in the following paragraphs.

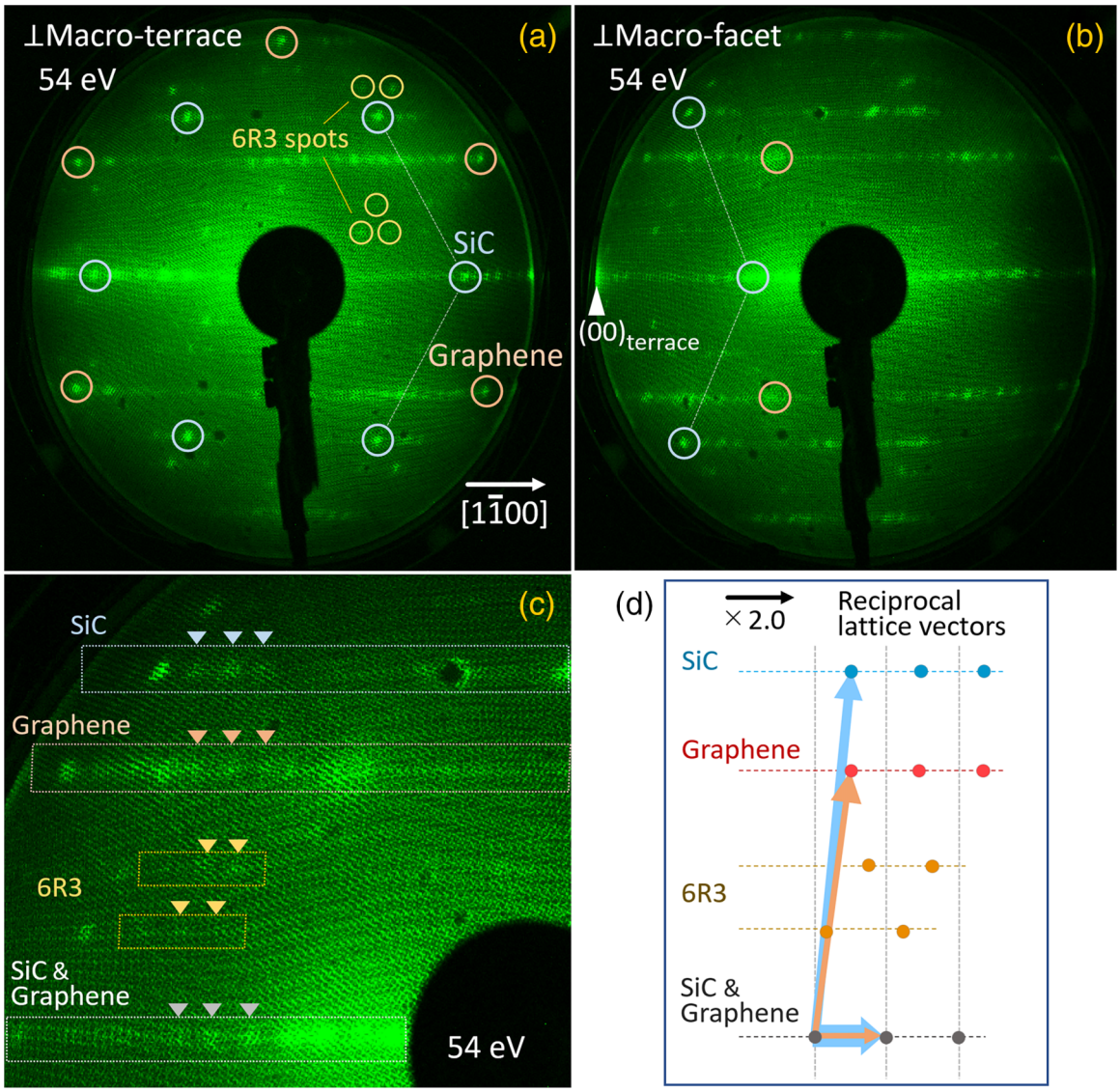

FIG. 2. Low-energy electron diffraction patterns, obtained with a beam incidence normal to (a) the macroterraces and (b) the macrofacets, with an electron energy of 54 eV. The thin blue dotted line indicates the same SiC reflexes on both patterns. (c) A zoomed portion of (b) showing the superspots of SiC, graphene, and the 6R3 structure. (d) Correspondence between some of the superspots shown in (c) for SiC, graphene, and the 6R3 structure superlattice; the horizontal scale is doubled.

The LEED measurements were performed at two different incident beam directions, that is, normal to the macroterraces and macrofacets. In the first case [Fig. 2(a)], besides the typical (1,0) spots of epitaxial graphene and SiC(0001) substrate and the satellite spots of the 6R3 buffer layer, chainlike superspots aligned along the [1$\bar{1}$00] direction were observed. When the incident electron energy was changed, these superspots moved not only toward the center of the LEED pattern, as other major spots did, but also slid along the [1$\bar{1}$00] direction; this indicates that they came from the areas not normal to the incident beam, i.e., from macrofacets and not from the macroterraces. Indeed, when the sample was rotated 27°, that is, when the beam was normal to the macrofacets, the movement of these superspots with varying of the electron energy became focused toward the pattern center [Fig. 2(b)]. As shown in Fig. 2(c), an enlarged view of Fig. 2(b), the chainlike superspots were observed around not only the main graphene spots, but also the SiC and 6R3 reflexes in this case. As will be discussed below, this was due to the moiré pattern between facet graphene and the SiC lattice along the [11$\bar{2}$0] direction. All the superspots were equidistant and indicated a real-space periodicity of ∼3.3 nm. Figure 2(d) shows a diagram of the reciprocal cells corresponding to the observed periodic structures on the macrofacets.

The macrofacets were then studied by STM. An STM topographic image measured at a tip bias voltage of 0.6 V (filled states) showed a bright and dark striped pattern along the [1$\bar{1}$00] direction [Fig. 3(a)]. A more detailed image of the region outlined by the red square taken at a lower bias of 0.3 V is shown in Fig. 3(b). A cross-sectional height profile along the gray line is shown in Fig. 3(c), indicating the overall periodicity of 3.3 nm, which coincides with the calculated one from spacing of the LEED superspots shown in Fig. 2. The corrugation is rather small at ∼0.8 Å. The valley

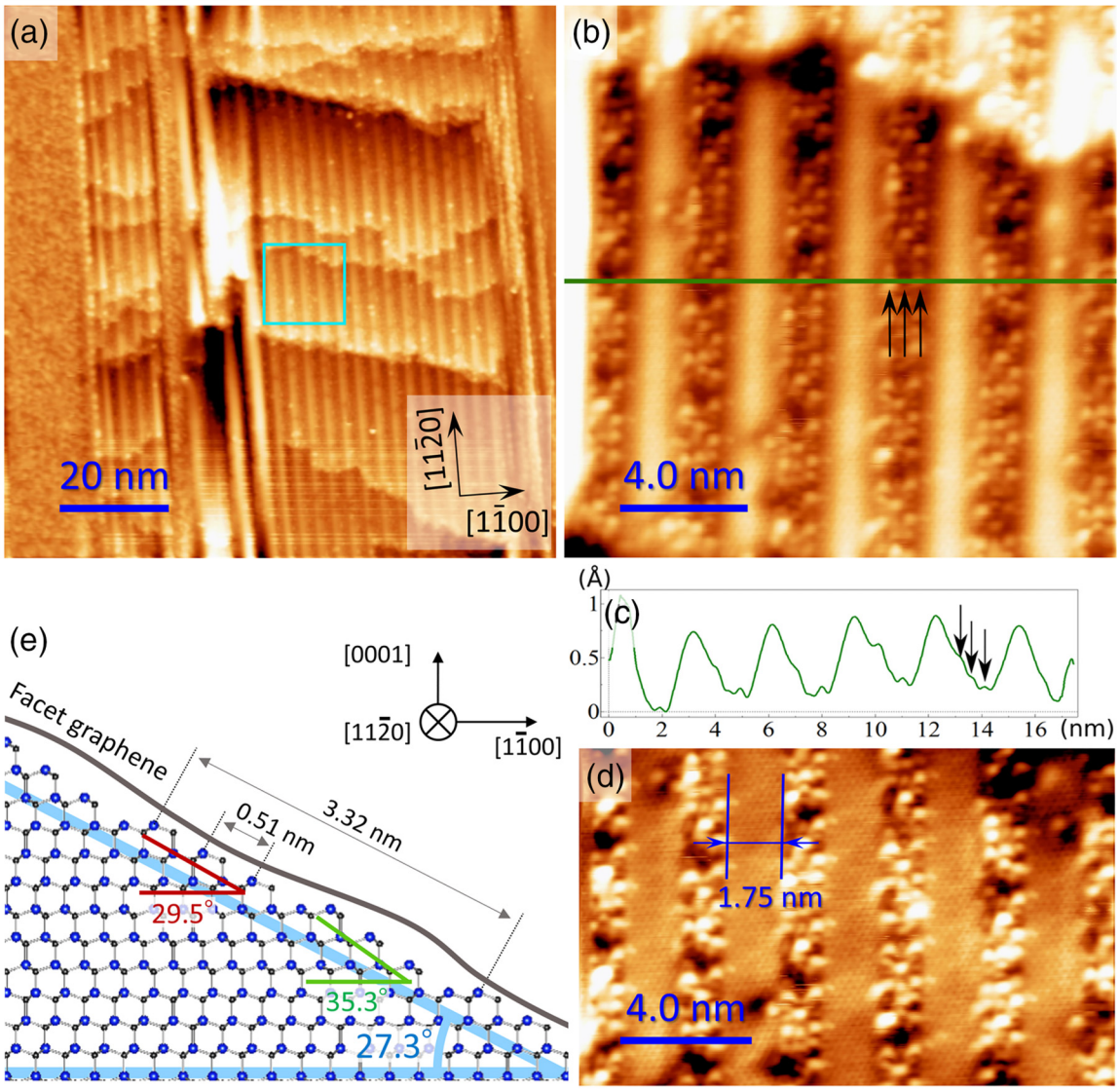

FIG. 3. (a) STM image of facet graphene on the macrofacet (100×100 nm^2, $V_t = 0.6$ V). (b) Enlarged area containing pseudo-GNRs (17×17 nm^2, $V_t = 0.3$ V). Three rows of protrusions in the buffer-layer-like region are highlighted by arrows. (c) Cross-sectional height profile along the gray line in (b). (d) STM image of the same area as in (b) with applied additional flattening along the x axis, so the atomically resolved graphene structure and edges of ribbons are more visible. (e) Cross-sectional atomic structural model of the macrofacets.

(darker) regions exhibited dotlike features lining up in the [11$\bar{2}$0] direction. The structure appears to have three rows of protrusions as indicated by arrows. Notably, as seen from the line profile in Fig. 3(c), protrusion rows are slightly inclined relative to the facet plane, causing this area to have $\sim$1.5° larger angle than the average 27° of the facet. In Fig. 3(d), the same structure is shown after flattening the image along the x axis to make atomically resolved features clearer. It is obvious that the valley areas with dotted features do not exhibit any graphene lattice appearance. Thus, it may be safely assumed that in these areas, the graphitic layer is bonded strongly to the substrate similarly to the 6R3 buffer layer. The bright ridge areas from Fig. 3(b), on the other hand, have a very distinguishable graphene lattice in the flattened image [Fig. 3(d)] in form of ribbons with extremely well-defined width of $\sim$1.7–1.8 nm and abrupt edge structure. The fact that the graphene lattice is so well resolved and lacks noticeable defects proves that these are high-quality GNRs.

Based on the AFM and STM results, we built a structure model of the macrofacet surface, having an average angle of 27.3° [Fig. 3(e)], which consists of miniterraces coupled with 35.3° and 29.5° minifacets, corresponding to the ridges and valleys, respectively, in the STM image. The overall period is 3.32 nm. These two characteristic minifacet angles arose because, in 6H-SiC(0001), a stacking sequence of Si-C bilayers is switched for every three of them, resulting in locally different facet angles relative to (0001). In the 29.5° minifacets, each row of carbon and silicon atoms is separated by 0.51 nm intervals, which is consistent with the dot-row spacing observed in the STM image in Fig. 3(b), and also in good correspondence with the STM deducted approximate angle of that minifacet (27.3° + 1.5° mentioned in the previous paragraph).

We further investigated the stability of each minifacet under monolayer graphene. The 29.5° and 35.3° minifacets contain two and one dangling bonds per carbon atom at the step edge, respectively, and thus are correspondingly more and less reactive to graphene. As a result, the graphene on each minifacet can exhibit different characteristics in both bonding configurations and electronic structure; these differences were indeed highlighted by the STM image shown in Fig. 3(d). A bufferlike graphitic layer was formed on the 29.5° minifacets while quasi-freestanding graphene, in the form of nanoribbons, grew on the 35.3° ones. Interestingly, 35.3° minifacets represent chunks of the *m*-plane SiC($1\bar{1}00$) surface, and previous study showed that graphene does not form a buffer layer on this surface [25]. In the following discussion, we define the bright and dark regions in Fig. 3(b) as pseudo-GNRs and buffer layer ribbons (BLRs), respectively. Here, we used the term pseudo-GNRs for our graphene nanostructures, which continuously connect to BLRs, to contrast the GNR term used for classical isolated nanoribbons.

One of the expected characteristic features of narrow GNRs is band-gap opening. Measurements of electronic properties of the carbon layer on facets by scanning probe techniques are challenging because of various parasitic interactions between the sides of the tip and facet surfaces. However, our STS measurements across periodic pseudo-GNR array structures show consistent periodic changes in the dI/dV spectra (particularly in values of the gap in the density of states), indicating the data are reproducible. The STS spectra have been measured in a number of closely located points across the facet. In Fig. 4(a), the blue curve shows the topography of the measured points. The points with larger height values are at bright ridge positions in Fig. 3(b) and correspond to the pseudo-GNR's location. In Fig. 4(b), the corresponding dI/dV spectra are shown. One may clearly observe the presence of a band gap in the density of states. The gap value is varying with good correlation to the measurement positions, as indicated by a red curve in Fig. 4(a). While the absolute measured value of the gap may be influenced by a number of experimental factors, it is clear that in ridge areas corresponding to the pseudo-GNR's location, the gap is noticeably larger. Thus, there would be no contradiction in the interpretation of this gap as one related to the nanoribbon nature. We estimate the GNR gap to be ~0.4–0.5 eV. The reduced apparent gap in the BLR regions is believed to originate from the localized states rather than band conductance as seen in overall STM appearance, and thus will not hinder isolation of pseudo-GNRs. It should also be noted here that even though the pseudo-GNR width appears fairly uniform as shown Fig. 3(d), there could be a slight variation in ribbon width due to defects or substrate interaction configurations. The band gap of such narrow GNR's is known to be extremely sensitive to even slight width variation [26]. This could be one of the reasons for the energy gap fluctuation in the localized STS measurements in Fig. 4(a).

The samples were successively investigated via micro-Raman spectroscopy. Given the difficulty in extracting the Raman spectrum of the facet graphene alone due to the limited spatial resolution (~1 μm) of the equipment used, we have analyzed two areas on the samples: one with a carbon layer covering the whole surface, i.e., both the macroterraces (in the form of the buffer layer [27,28]) and macrofacets, and the other with a carbon layer only on the macroterraces but not on macrofacets [as shown in Fig. 1(c), such areas could easily be identified by phase AFM] [Fig. 5(b)]. Figure 5(a) shows the measured spectra of both areas and the one of the facet graphene alone, obtained by subtracting the blue spectrum from the red one. A Raman spectrum of graphene usually shows the *D*, *G*, and 2*D* peaks. In this study, the 2*D* peak, which is originated from the double resonance two-phonon inelastic scattering [29], was absent. In the case of a narrow GNR with armchair edge, however, double inelastic scattering (with the wave vector directed across the ribbon width) is much less probable than elastic scattering by the edges, rendering the 2*D* peak almost negligible and the *D* peak relatively high. This phenomenon has also been observed in other GNRs [30,31]. Thus, the absence of the 2*D* peak suggests that in our case, pseudo-GNRs indeed behave similarly to narrow armchair GNRs. In the *D* and *G* regions, three peak components could be recognized [Fig. 5(a)].

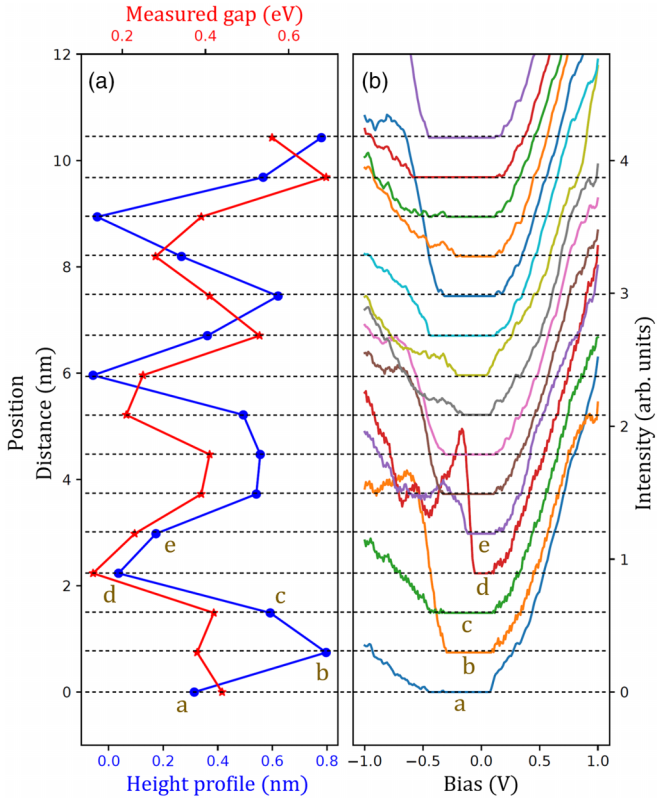

FIG. 4. STS data taken along the line across the minifacet [same area as in Fig. 3(b)]. (a) The height of the point where the STS spectra were recorded (blue) and the measured band gap (red). (b) Corresponding STS spectra.

To better understand the spectral features, higher-resolution spectra were also measured at $\theta = 0°$ and $\theta = 90°$, that is, with light polarization parallel and perpendicular to the pseudo-GNR edges, respectively [Figs. 5(c) and 5(d)], revealing the light polarization dependence of the Raman spectra of facet graphene. The experimental spectra were fitted with six Lorentzian peaks, which were categorized into three origins: GNRs, BLRs, and an unknown component. The peaks having BLR origin were identified since their positions

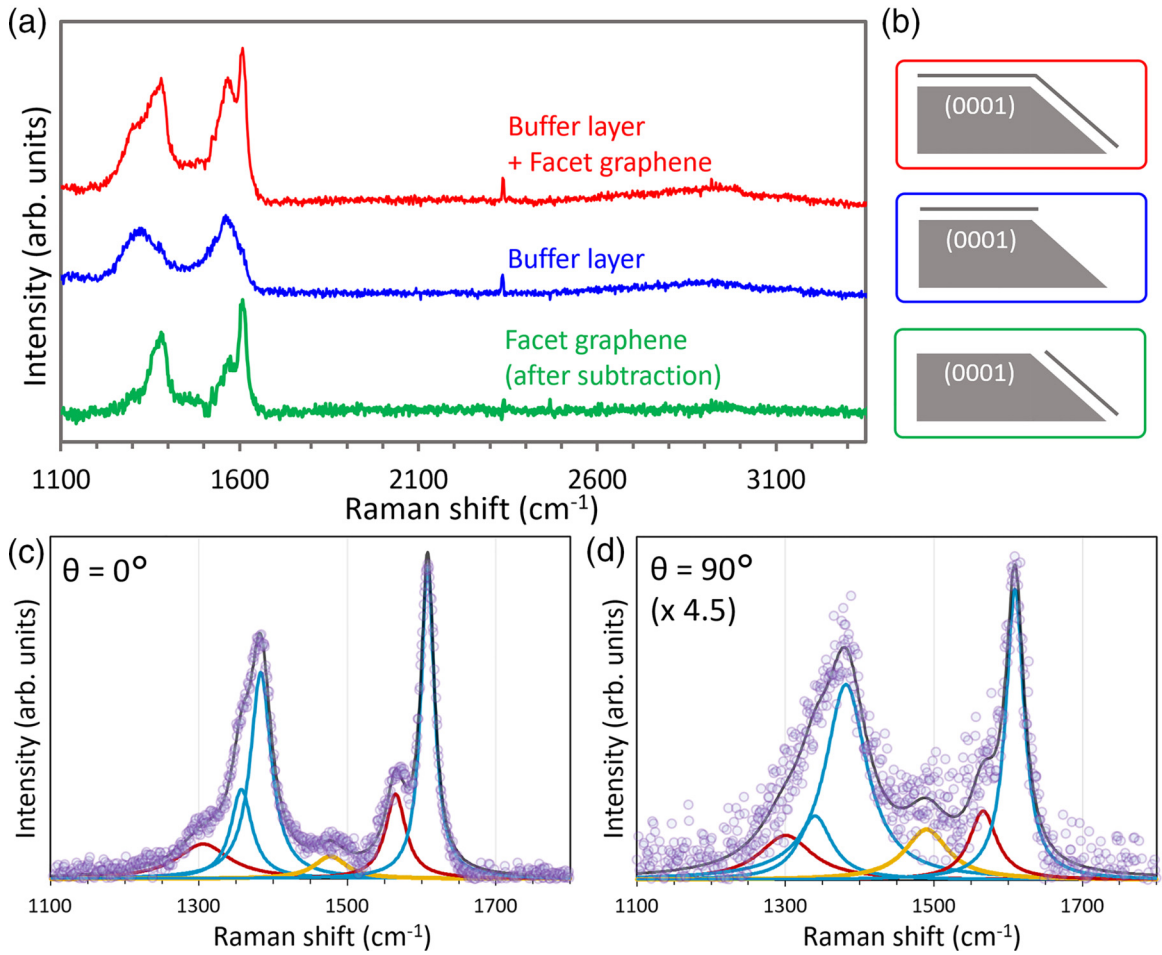

FIG. 5. (a) Raman spectra of the regions covered entirely by a carbon layer (red), only buffer layer on macroterraces (blue), and their difference (green) corresponding to the Raman spectrum of the carbon layer on macrofacets. (b) Cross-sectional schematic views of the sample whose spectra are shown in (a). (c),(d) Extracted Raman spectra of facet graphene, measured with light polarization that is (c) parallel and (d) perpendicular to the pseudo-GNR edge; the intensity of data in (d) is ×4.5 smaller than that in (c). The lilac circles represent the measured values, the blue and red peaks correspond to the pseudo-GNR and buffer layer ribbon regions in facet graphene, respectively, and the solid black line is the total fit curve (the origin of the yellow peak is still unclear).

approximately matched the peaks in the 6R3 buffer layer on (0001) macroterraces observed in the blue spectrum in Fig. 5(a); they were attributed to a carbon sheet with sp^3 bondings of BLRs (similarly to the 6R3 structure). The origin of the yellow peak at ∼1500 cm^{-1} was difficult to identify, but it may be associated with the edge mode [32,33]. The curve with GNR origin consisted of three peaks: one *G* peak at ∼1610 cm^{-1} and two *D* peaks at ∼1370 cm^{-1}. The latter ones were probably due to either the bulk- and edge-phonon contributions or the phonon energy difference depending on the scattering schemes for the *D*-band transition. The *G* peak was at a higher wave number compared to that for pristine graphene (∼1580 cm^{-1}) reported by Lee *et al.* [34]. We could not determine the cause of this blueshift, but it may be due to compressive strain, hole doping, or band-gap opening [34–36]. Band-gap opening is the most plausible cause since our pseudo-GNRs were 2 nm wide and of the armchair-edge type, which should result in a band gap larger than 0.4 eV, based on the theoretical GNR calculations [26].

Finally, the polarization dependence shown in Figs. 5(c) and 5(d) indicates that the spectra at each angle were similar in shape, but an intensity is reduced by 1/4.5. This is a typical feature of armchair-edge graphene [37,38]. All the Raman spectroscopy results described above confirm the formation of pseudo-GNR arrays on the macrofacets.

IV. CONCLUSIONS

We have studied graphitization phenomena on the macrofacets formed during thermal decomposition of vicinal 6*H*-SiC(0001) surfaces with a relatively large miscut angle (∼15°) toward the [1$\bar{1}$00] direction. The step bunching and graphitization resulted in the formation of the macrofacets inclined by 27° with respect to the (0001). Monolayer carbon was formed on the macrofacet surface and sectioned by pseudo-GNR and BLR areas due to the periodically striped surface structure. An array of aligned pseudo-GNRs, each one having a width of ∼1.7 nm and being lined up with a 3.3 nm period, was identified. The parameters of the pseudo-GNR array appear to be solely dependent on the SiC polytype and not on the substrate miscut angle. The quality and overall size

of the array can be regulated by the proper choice of substrate conditions.

An indicated 0.4–0.5 eV energy gap measured by STS, the polarization dependence of the G and D peaks, and the absence of the $2D$ peak by Raman spectroscopy confirms that pseudo-GNRs exhibit properties of armchair-edge GNRs with narrow width. The pseudo-GNRs were separated by BLRs, which implies that they were electronically isolated. The very high uniformity, density, ideal alignment, high structural quality, and very narrow width of the pseudo-GNRs array on a semiconductor substrate created via the simple annealing process open up unique possibilities for applications in next-generation electronics.

[1] A. K. Geim and K. S. Novoselov, The rise of graphene, Nat. Mater. **6**, 183 (2007).

[2] K. S. Novoselov, Z. Jiang, Y. Zhang, S. V. Morozov, H. L. Stormer, U. Zeitler, J. C. Maan, G. S. Boebinger, P. Kim, and A. K. Geim, Room-temperature quantum Hall effect in graphene, Science **315**, 1379 (2007).

[3] K. Nakada, M. Fujita, G. Dresselhaus, and M. S. Dresselhaus, Edge state in graphene ribbons: Nanometer size effect and edge shape dependence, Phys. Rev. B **54**, 17954 (1996).

[4] K. Wakabayashi, M. Fujita, H. Ajiki, and M. Sigrist, Electronic and magnetic properties of nanographite ribbons, Phys. Rev. B **59**, 8271 (1999).

[5] M. Y. Han, B. Özyilmaz, Y. Zhang, and P. Kim, Energy Band-Gap Engineering of Graphene Nanoribbons, Phys. Rev. Lett. **98**, 206805 (2007).

[6] L. Jiao, L. Zhang, X. Wang, G. Diankov, and H. Dai, Narrow graphene nanoribbons from carbon nanotubes, Nature (London) **458**, 877 (2009).

[7] L. Talirz, H. Söde, T. Dumslaff, S. Wang, J. R. Sanchez-Valencia, J. Liu, P. Shinde, C. A. Pignedoli, L. Liang, V. Meunier *et al.*, On-surface synthesis and characterization of 9-atom wide armchair graphene nanoribbons, ACS Nano **11**, 1380 (2017).

[8] J. Cai, P. Ruffieux, R. Jaafar, M. Bieri, T. Braun, S. Blankenburg, M. Muoth, A. P. Seitsonen, M. Saleth, X. Feng *et al.*, Atomically precise bottom-up fabrication of graphene nanoribbons, Nature (London) **466**, 470 (2010).

[9] T. Kajiwara, Y. Nakamori, A. Visikovskiy, T. Iimori, F. Komori, K. Nakatsuji, K. Mase, and S. Tanaka, Graphene nanoribbons on vicinal SiC surfaces by molecular beam epitaxy, Phys. Rev. B **87**, 121407(R) (2013).

[10] J. Baringhaus, F. Edler, and C. Tegenkamp, Edge-states in graphene nanoribbons: A combined spectroscopy and transport study, J. Phys.: Condens. Matter **25**, 392001 (2013).

[11] J. Baringhaus, M. Ruan, F. Edler, A. Tejeda, M. Sicot, A. Taleb-Ibrahimi, A.-P. Li, Z. Jiang, E. H. Conrad, C. Berger *et al.*, Exceptional ballistic transport in epitaxial graphene nanoribbons, Nature (London) **506**, 349 (2014).

[12] A. L. Miettinen, M. S. Nevius, W. Ko, M. Kolmer, A.-P. Li, M. N. Nair, B. Kierren, L. Moreau, E. H. Conrad, and A. Tejeda, Edge states and ballistic transport in zigzag graphene ribbons: The role of SiC polytypes, Phys. Rev. B **100**, 045425 (2019).

[13] A. A. Zakharov, N. A. Vinogradov, J. Aprojanz, T. T. N. Nguyen, C. Tegenkamp, C. Struzzi, T. Iakimov, R. Yakimova, and V. Jokubavicius, Wafer scale growth and characterization of edge specific graphene nanoribbons for nanoelectronics, ACS Appl. Nano Mater. **2**, 156 (2019).

[14] I. Palacio, A. Celis, M. N. Nair, A. Gloter, A. Zobelli, M. Sicot, D. Malterre, M. S. Nevius, W. A. de Heer, C. Berger *et al.*, Atomic structure of epitaxial graphene sidewall nanoribbons: Flat graphene, miniribbons, and the confinement gap, Nano Lett. **15**, 182 (2015).

[15] M. S. Nevius, F. Wang, C. Mathieu, N. Barrett, A. Sala, T. O. Mentes, A. Locatelli, and E. H. Conrad, The bottom-up growth of edge specific graphene nanoribbons, Nano Lett. **14**, 6080 (2014).

[16] N. Camara, J.-R. Huntzinger, G. Rius, A. Tiberj, N. Mestres, F. Pérez-Murano, P. Godignon, and J. Camassel, Anisotropic growth of long isolated graphene ribbons on the C face of graphite-capped 6H-SiC, Phys. Rev. B **80**, 125410 (2009).

[17] H. Nakagawa, S. Tanaka, and I. Suemune, Self-Ordering of Nanofacets on Vicinal SiC Surfaces, Phys. Rev. Lett. **91**, 226107 (2003).

[18] M. Fujii and S. Tanaka, Ordering Distance of Surface Nanofacets on Vicinal 4H-SiC(0001), Phys. Rev. Lett. **99**, 016102 (2007).

[19] T. Kimoto, A. Itoh, and H. Matsunami, Step bunching in chemical vapor deposition of 6H- and 4H-SiC on vicinal SiC(0001) faces, Appl. Phys. Lett. **66**, 3645 (1995).

[20] T. Kimoto, A. Itoh, and H. Matsunami, Step bunching mechanism in chemical vapor deposition of 6H- and 4H-SiC{0001}, J. Appl. Phys. **81**, 3494 (1997).

[21] K. Ienaga, T. Iimori, K. Yaji, T. Miyamachi, S. Nakashima, Y. Takahashi, K. Fukuma, S. Hayashi, T. Kajiwara, A. Visikovskiy *et al.*, Modulation of electron-phonon coupling in one-dimensionally nanorippled graphene on a macrofacet of 6H-SiC, Nano Lett. **17**, 3527 (2017).

[22] K. V. Emtsev, F. Speck, T. Seyller, L. Ley, and J. D. Riley, Interaction, growth, and ordering of epitaxial graphene on SiC0001 surfaces: A comparative photoelectron spectroscopy study, Phys. Rev. B **77**, 155303 (2008).

[23] S. Kim, J. Ihm, H. J. Choi, and Y.-W. Son, Origin of Anomalous Electronic Structures of Epitaxial Graphene on Silicon Carbide, Phys. Rev. Lett. **100**, 176802 (2008).

[24] F. Varchon, P. Mallet, J.-Y. Veuillen, and L. Magaud, Ripples in epitaxial graphene on the Si-terminated SiC(0001) surface, Phys. Rev. B **77**, 235412 (2008).

[25] M. Ostler, I. Deretzis, S. Mammadov, F. Giannazzo, G. Nicotra, C. Spinella, Th. Seyller, and A. La Magna, Direct growth of quasi-free-standing epitaxial graphene on nonpolar SiC surfaces, Phys. Rev. B **88**, 085408 (2013).

[26] Y.-W. Son, M. L. Cohen, and S. G. Louie, Energy Gaps in Graphene Nanoribbons, Phys. Rev. Lett. **97**, 216803 (2006).

[27] F. Fromm, M. H. Oliveira Jr., A. Molina-Sànchez, M. Hundhausen, J. M. J. Lopes, H. Riechert, L. Wirtz, and T. Seyller, Contribution of the buffer layer to the Raman spectrum of epitaxial graphene on SiC(0001), New J. Phys. **15**, 043031 (2013).

[28] W. Strupinski, K. Grodecki, P. Caban, P. Ciepielewski, I. Jozwik-Biala, and J. M. Baranowski, Formation mechanism of graphene buffer layer on SiC(0001), Carbon **81**, 63 (2015).

[29] L. G. Cançado, M. A. Pimenta, R. Saito, A. Jorio, L. O. Ladeira, A. Grueneis, A. G. Souza-Filho, G. Dresselhaus, and M. S. Dresselhaus, Stokes and anti-Stokes double resonance Raman scattering in two-dimensional graphite, Phys. Rev. B **66**, 035415 (2002).

[30] R. Yang, Z. Shi, L. Zhang, D. Shi, and G. Zhang, Observation of Raman G-peak split for graphene nanoribbons with hydrogen-terminated zigzag edges, Nano Lett. **11**, 4083 (2011).

[31] A. N. Sokolov, F. L. Yap, N. Liu, K. Kim, L. Ci, O. B. Johnson, H. Wang, M. Vosgueritchian, A. L. Koh, J. Chen *et al.*, Direct growth of aligned graphitic nanoribbons from a DNA template by chemical vapour deposition, Nat. Commun. **4**, 2402 (2013).

[32] R. Saito, M. Furukawa, G. Dresselhaus, and M. S. Dresselhaus, Raman spectra of graphene ribbons, J. Phys.: Condens. Matter **22**, 334203 (2010).

[33] W. Ren, R. Saito, L. Gao, F. Zheng, Z. Wu, B. Liu, M. Furukawa, J. Zhao, Z. Chen, and H.-M. Cheng, Edge phonon state of mono- and few-layer graphene nanoribbons observed by surface and interference co-enhanced Raman spectroscopy, Phys. Rev. B **81**, 035412 (2010).

[34] J. E. Lee, G. Ahn, J. Shim, Y. S. Lee, and S. Ryu, Optical separation of mechanical strain from charge doping in graphene, Nat. Commun. **3**, 1024 (2012).

[35] K. Sasaki, K. Kato, Y. Tokura, S. Suzuki, and T. Sogawa, Decay and frequency shift of both intervalley and intravalley phonons in graphene: Dirac-cone migration, Phys. Rev. B **86**, 201403(R) (2012).

[36] R. Gillen, M. Mohr, C. Thomsen, and J. Maultzsch, Vibrational properties of graphene nanoribbons by first-principles calculations, Phys. Rev. B **80**, 155418 (2009).

[37] K. Sasaki, R. Saito, K. Wakabayashi, and T. Enoki, Identifying the orientation of edge of graphene using G band Raman spectra, J. Phys. Soc. Jpn. **79**, 044603 (2010).

[38] L. G. Cançado, M. A. Pimenta, B. R. A. Neves, M. S. S. Dantas, and A. Jorio, Influence of the Atomic Structure on the Raman Spectra of Graphite Edges, Phys. Rev. Lett. **93**, 247401 (2004).